

Electronic structure and magnetic properties of Ni_{3n}Al_n clustersVaishali Shah^{1,*} and D. G. Kanhere^{2,3}¹*Institute of Bioinformatics and Biotechnology, University of Pune, Pune 411 007, India*²*Department of Physics, University of Pune, Pune 411 007, India*³*Centre for Modeling and Simulation, University of Pune, Pune 411 007, India*

(Received 8 May 2009; revised manuscript received 13 August 2009; published 21 September 2009)

The equilibrium structure, electronic, and magnetic properties of Ni_{3n}Al_n ($n=1, 8$) clusters are investigated using *ab initio* total-energy calculations based on density functional theory. Asymmetric and amorphous structures are observed for $n > 1$ clusters, in contrast with the earlier work reported based on Gupta potentials; where, clusters with Ni₃Al compositions were found to be symmetric. Magnetic moment per atom in these clusters is significantly enhanced with respect to the bulk. The distribution of magnetic charge on Ni and Al atoms is highly inhomogeneous and depends on their number of Al and Ni neighbors. The Al atoms quench the magnetic moments of Ni_{3n}Al_n clusters when compared with the magnetic moments of pure Ni clusters. The analysis of the charge density shows a net transfer of charge from *s*-type orbital of Ni to *p*-type orbital of Al. The density of states exhibits features like Heusler alloys. The implications of this on the conductance in such clusters are discussed.

DOI: [10.1103/PhysRevB.80.125419](https://doi.org/10.1103/PhysRevB.80.125419)

PACS number(s): 73.22.-f, 71.15.Mb, 75.50.Cc, 75.75.+a

I. INTRODUCTION

Since the last three decades, there is an ever growing interest in investigating homoatomic and heteroatomic nanoclusters by experimental and theoretical methods. The significantly different properties of the nanoclusters, in comparison with their atomic and bulk forms are being used for applications in various fields like physics, chemistry, materials science, and biology. Within nanoclusters, the properties often differ as a function of their size.¹ The structure and properties of bimetallic clusters depend not only on the size, but also on the composition of the bimetallic alloy mixture and play an important role in tuning the chemical, physical, optical, and magnetic properties. Such clusters are thus attractive for controlling specific properties, by harnessing the diversity of compositions that becomes available.

The structural, electronic, and magnetic properties of the simplest nanoalloy clusters, namely, bimetallic clusters have been investigated using different theoretical and experimental techniques. One such bimetallic nanoalloy that has been of interest in cluster studies is NiAl. NiAl is one of the nickel-based superalloys used in advanced material technology. Within the various nickel-based superalloys, Ni₃Al alloy has been of particular interest on account of better oxidation resistance, corrosion resistance, and thermal fatigue resistance.^{2,3} Ni₃Al alloy has an ordered crystal structure of L1₂ type.⁴ Clusters of varying size and compositions of NiAl have been investigated earlier with semiempirical many-body potentials.⁵⁻⁹ Such theoretical calculations based on model interaction potentials are computationally less expensive. Their results are quantitatively less accurate, but qualitatively reasonable. In some cases, a major drawback of the model empirical potentials is that, results using different interatomic potentials often differ, and may even contradict each other. For example, Al atom is predicted to occupy the central position of a symmetric icosahedron in the ground-state structure of Ni₁₂Al cluster by Krissinel and Jellinek,⁶ whereas, Rey *et al.* predicted that the central position will be

occupied by Ni atom with Al located on the surface of a slightly distorted icosahedron.⁵ Such differences in predictions leave unanswered questions and underline the necessity of more reliable and accurate methods of investigations. The density functional theory (DFT)-based calculations by Calleja *et al.* predict the structure of Ni₁₂Al to be a Jahn-Teller distorted asymmetric icosahedron with the larger Al atom residing at the cluster surface.¹⁰ They have argued that the Al atom prefers to segregate to the surface of the cluster on account of Al atoms having a lower surface energy as compared with Ni. Further, surface segregation of Al atoms prevents the cluster from undergoing an expansion, which reduces the surface energy of the cluster. Thus, the geometry of the Ni₁₂Al cluster is not driven by maximizing the Ni-Al bonds, which would be the case if Al atoms occupy a central position but by reducing the energy of the Ni-Ni bonds.

In spite of being qualitatively accurate, there are a limited number of DFT-based investigations on bimetallic clusters because of their demand of high computational resources. Several first-principles studies on homoatomic clusters of small Ni (Refs. 11–21) and Al (Refs. 22–27) have been performed. However, investigations on NiAl clusters, using first-principles total-energy calculations have been limited to a few case study clusters like dimers, trimers, tetramers, and Ni₁₂Al.^{10,28} Recently, the structure and stability of clusters of Ni-Al with varying size and compositions have been studied using a genetic algorithm approach in combination with Gupta potentials by Bailey *et al.*²⁹ They investigated as a part of their study, clusters with total number of atoms ≥ 20 and having an approximate composition of Ni₃Al. Their investigations show that such clusters with an approximate composition of Ni₃Al have icosahedral packing until 34 atoms and octahedral packing until 38 atoms. The lowest-energy isomer structure of these clusters is dominated by the maximization of the number of Ni-Al interactions.

As demonstrated by Calleja *et al.*, the *ab initio* calculations on Ni-Al clusters being quantitatively accurate, are able to determine the positions of atoms in a bimetallic alloy nanocluster more reliably.¹⁰ Such calculations are capable of

taking into account the Jahn-Teller distortions in the structural configurations of many-body systems. Yao *et al.* investigated the size dependence of magnetic moments of nanoclusters and have indicated the importance of proper structural optimization for determining the magnetic properties of Ni_n ($n=13 \sim 56$) clusters.³⁰ A systematic investigation based on density functional method of the structural properties of nanoclusters of the Ni_3Al alloy composition is hence crucial. We believe, such calculations play an important role in validating the usefulness of empirical potentials for determining the structures of small clusters of bimetallic alloys in different composition ratios. To our knowledge, no investigations based on an *ab initio* total-energy approach, are available for small clusters with Ni_3Al composition.

Theoretical simulations by various authors show that pure clusters of Ni^{16,17,30} as well as Al (Refs. 27 and 31) follow an icosahedral packing growth pattern. In the case of mixed clusters, it is interesting to look at the following questions using the first-principles method of investigation: (1) do clusters of 3:1 composition ratio of NiAl follow a growth pattern based on icosahedral or double-icosahedral packing? (2) With bulk Ni_3Al known to have an ordered L_{12} structure, do small clusters of the same elemental composition ratio show symmetry and ordering? (3) Will Al occupy a position at the center of the clusters or segregate to the surface? Besides the structural properties, it is also interesting to understand the magnetic properties of these clusters. An understanding of the distribution of magnetic charges in clusters made up of magnetic and nonmagnetic elements is interesting for various technological applications.

This paper is organized as follows: details of the computational procedure used in our study are described briefly in Sec. II. In Sec. III, we present and discuss our results and in Sec. IV, we summarize our main conclusions.

II. COMPUTATIONAL DETAILS

In order to determine the ground-state structure and magnetic properties of the $\text{Ni}_{3n}\text{Al}_n$, ($n=1, 8$) clusters, we have performed DFT-based total-energy calculations using the Vienna *Ab Initio* Simulation Package (VASP).³² All the core-valence electron interactions were described by ultrasoft pseudopotentials,³³ and the exchange and correlation energy using the PW91 generalized gradient approximation (GGA). The choice of exchange and correlation energy functional was determined by performing bulk calculations on Ni_3Al . The calculated bulk lattice parameter of 3.58 Å is in good agreement with the experimental value of 3.568 Å.³⁴ The kinetic energy cutoff of 17.76 Ry was found to be sufficient for convergence. The simulation unit cell for each cluster was chosen so that a vacuum spacing of at least 8 Å exists in each direction. The 3s, 3p for Al and 3d, 4s orbitals for Ni were treated as valence states. Geometry optimizations are performed using conjugate gradient method and residual minimization method with direct inversion in the iterative subspace, until all force components on each atom are less than the 10^{-3} eV/Å.

The initial configurations of the $\text{Ni}_{3n}\text{Al}_n$, ($n=1, 8$) clusters are generated using a combination of classical and *ab initio*

molecular dynamics so as to maximize the exploration of the configurational space. The initial sampling of the configurational space is performed using the XMD (Ref. 35) molecular dynamics program with the many-body interactions described by Gupta potential.³⁶ Several configurations corresponding to local minima in the potential energy are chosen as initial configurations for minimization by VASP. In addition, we have carried out constant-temperature molecular dynamics run at 2000 K using VASP. The cluster is thermalized at this temperature and allowed to explore the phase space for 70–100 ps. Several initial configurations are chosen from this thermalization run. For each of the clusters, we have optimized 40 distinct initial configurations using VASP with a convergence in the total energy on the order of 10^{-4} eV. The three lowest-energy structures were subsequently chosen for noncollinear spin-polarized density functional calculations and the ground-state structures were determined. The equilibrium structures did not depict any noncollinearity in the magnetization vectors.

The binding energy per atom of the ground-state clusters is calculated as

$$\text{B.E.} = \frac{1}{N} [E_{\text{Ni}_{3n}\text{Al}_n} - n(3E_{\text{Ni}} - E_{\text{Al}})], \quad (1)$$

where, N is the total size of the cluster and n refers to the multiples of Ni_3Al in a particular cluster. The local magnetic moment M at each site can be calculated as

$$M = \int_0^R [\rho^\uparrow(\mathbf{r}) - \rho^\downarrow(\mathbf{r})] d\mathbf{r}, \quad (2)$$

where, $\rho^\uparrow(\mathbf{r})$ and $\rho^\downarrow(\mathbf{r})$ are spin-up and spin-down charge densities, respectively, and R is the radius of the sphere centered at the atom. R for Ni and Al is chosen separately, taking into account the different sizes of these two atoms, so that there is no overlap between the spheres.

III. RESULTS AND DISCUSSION

A. Structural Properties

In this section, we discuss the structure of $\text{Ni}_{3n}\text{Al}_n$, ($n=1, 8$) clusters. The ground-state geometry of $\text{Ni}_{3n}\text{Al}_n$, ($n=1, 5$) clusters along with their isomers is presented in Fig. 1 For all the clusters, the ground-state structures, the first and the second isomer (wherever applicable) are marked (a), (b), and (c), respectively. The ground-state configuration of the smallest cluster, Ni_3Al is a regular tetrahedron with the Ni-Ni bond lengths of 2.25 Å and the three Ni-Al bond lengths are 2.40 Å. The other low-lying isomer has a planar configuration and lies 0.03 eV above the ground-state structure. The ground-state structure, as well as the low-lying isomers of Ni_6Al_2 , are bicapped distorted octahedron. The distorted octahedron is comprised of Ni_4Al_2 , with the remaining two Ni atoms tetrahedrally bonded to the faces of the distorted octahedron. There are eight possible sites for the two Ni atoms to bond tetrahedrally with the distorted octahedron of Ni_4Al_2 . The position of the remaining two Ni atoms in bonding with Ni_4Al_2 , determines the ground-state and the isomer structures. There are three equivalent isomers [only one structure

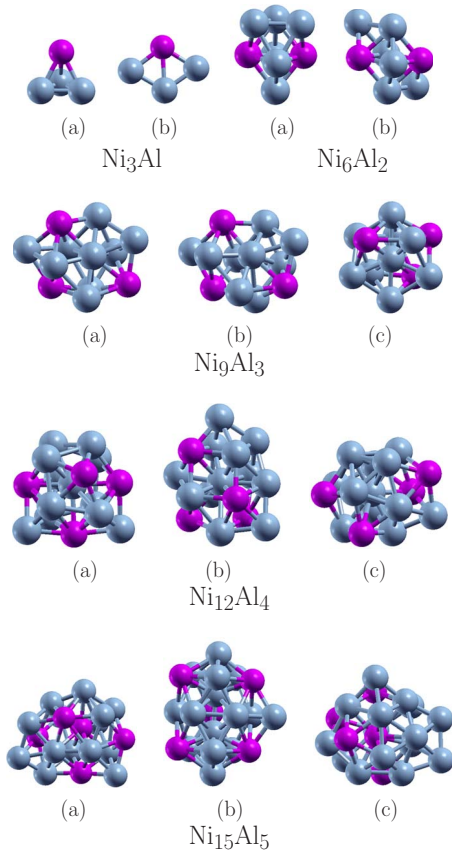


FIG. 1. (Color online) Ground-state structures of $\text{Ni}_{3n}\text{Al}_n$, ($n = 1, 5$) clusters with their two low-lying isomers. (a) represents the ground state, (b) indicates the first isomer and (c) indicates the second isomer structure. Grey spheres represent Ni atoms and purple spheres represent Al atoms.

is shown in (b)] that lie 0.06 eV above the ground-state structure.

The ground state of Ni_9Al_3 is a distorted asymmetric structure, comprised of tetrahedrally bonded units of Ni and Al. Majority of the tetrahedrons are comprised of three Ni and one Al atom. A degenerate isomer lies 0.0001 eV above the equilibrium state structure. A slightly asymmetric, incomplete icosahedron, lies 0.14 eV above the ground-state configuration. A symmetric, incomplete icosahedral geometry on optimization lead to the asymmetric, incomplete icosahedral structure.

The ground-state and isomer structures of $\text{Ni}_{12}\text{Al}_4$ are amorphous, with distorted tetrahedral and octahedral structures formed of Ni and Al atoms. There are two isomers at 0.18 and 0.32 eV above the equilibrium structure. The ground state and second isomer of $\text{Ni}_{15}\text{Al}_5$ are amorphous, and comprised of distorted tetrahedrons. The first isomer of $\text{Ni}_{15}\text{Al}_5$ lies at 0.03 eV above the ground state, and is seen to be a distorted double icosahedron, with a Ni atom capping around the waist. This structure has been reported to be the ground state, using genetic algorithm and Gupta potential-based calculations by Bailey *et al.*²⁹ Structure optimization performed by starting with a symmetric, double icosahedron lead to the distorted double icosahedral structure, that is, higher in energy with respect to the ground-state geometry of

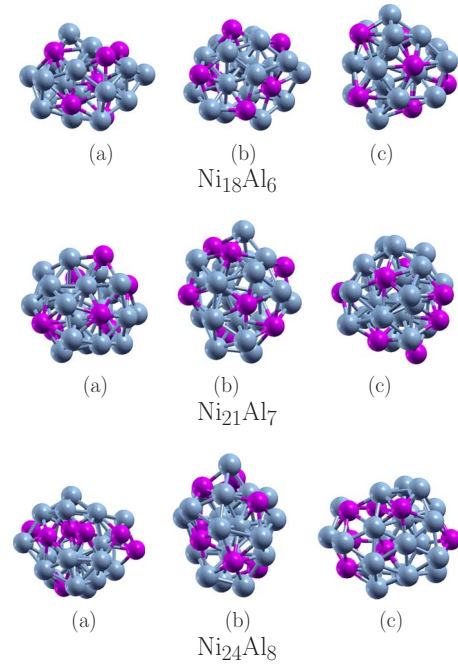


FIG. 2. (Color online) Ground-state geometries of $\text{Ni}_{3n}\text{Al}_n$, ($n = 6, 8$) clusters with their two isomers. (a) represents the ground state, (b) indicates the first isomer and (c) indicates the second isomer structure. Grey spheres represent Ni atoms and purple spheres represent Al atoms.

the cluster. The second isomer of $\text{Ni}_{15}\text{Al}_5$ is 0.3 eV above the ground-state geometry. $\text{Ni}_{15}\text{Al}_5$ is the first cluster to show a single Al atom trapped inside the cluster in both the ground-state and the second isomer structure.

The ground-state structure and low-lying isomers of $\text{Ni}_{3n}\text{Al}_n$, ($n=6, 8$), shown in Fig. 2, are also observed to be highly amorphous. For all the three clusters the ground-state structures are marked (a), the first and the second isomer are shown in (b) and (c), respectively. The structures of the ground-state geometry, as well as the two isomers of these three clusters, are cage-like and comprised of distorted pentagonal and hexagonal rings. Most of the distorted pentagonal and hexagonal rings are comprised of both Ni and Al atoms. Like the ground state of $\text{Ni}_{15}\text{Al}_5$, an Al atom is trapped inside the ground-state structure of $\text{Ni}_{18}\text{Al}_6$. The two isomers of $\text{Ni}_{18}\text{Al}_6$ are at 0.05 and 0.19 eV, respectively. The ground-state and isomer structures of $\text{Ni}_{21}\text{Al}_7$ show that, all Al atoms are distributed on the surface with no Al trapped inside. The two isomers of $\text{Ni}_{21}\text{Al}_7$ are at 0.26 and 0.35 eV, respectively. In $\text{Ni}_{24}\text{Al}_8$, no Al is observed to be trapped inside the equilibrium structure and the first isomer structure which lies 0.12 eV above it. The second isomer of $\text{Ni}_{24}\text{Al}_8$ lies at 0.18 eV and shows that one Al is trapped inside the cluster.

Our investigations show that the structures of $\text{Ni}_{3n}\text{Al}_n$, ($n=5, 8$) clusters are significantly different than those obtained by Gupta potential.²⁹ None of the structures have the distorted, double icosahedral centers capped around the waist,²⁹ except for the first isomer of $\text{Ni}_{15}\text{Al}_5$. The most significant feature in the structures of these clusters is that tetrahedral, pentagonal and hexagonal motifs are mostly com-

prised of both Ni and Al atoms. This intermixing of Ni and Al atoms in the structures leads to significant distortions in such small finite systems.

The key features observed in all the ground-state geometries of $\text{Ni}_{3n}\text{Al}_n$, ($n=1, 8$) clusters are, namely,

(1) except for Ni_3Al , which has a regular geometry, all clusters are either distorted symmetries or amorphous geometries.

(2) Al atoms prefer to segregate to the surface of the clusters.

(3) The Al atoms prefer to bond with maximum number of Ni atoms in agreement with the empirical potential calculations.²⁹

(4) An Al atom is seen to be trapped inside the cluster in the ground state of $\text{Ni}_{15}\text{Al}_5$ and $\text{Ni}_{18}\text{Al}_6$ only. However, this trend is not continued for the larger clusters investigated here.

(5) Clustering of Al atoms, either at the center or at the surface, is not energetically preferred.

(6) With increasing size of the clusters, systematic evolution patterns like capped icosahedron or capped double icosahedron are absent in the geometries of these clusters.

A detailed investigation of the geometries of the $\text{Ni}_{3n}\text{Al}_n$, ($n=2, 6$) clusters reveals that the distorted, asymmetric, and amorphous structures are energetically preferred over other low-lying structures, as the number of Ni-Al bonds in these structures is maximized, whereas, at the same time the number of Ni-Ni bonds is minimized. Our calculations on the Ni_3Al , Ni, and Al bulk systems show that their cohesive energies are 5.04, 4.94, and 3.43 eV, respectively. So cluster geometries with maximum number of Ni-Al bonds and minimum number of Ni-Ni and Al-Al bonds will be energetically more stable. The strength of Ni-Ni interactions being more than that of Al-Al interactions, besides an increase in the Ni-Al coordination, an increase in the Ni-Ni coordination over Al-Al coordination will be preferred. This also explains why most of the pentagonal and hexagonal motifs in the clusters are made up of both Ni and Al. Based on the number of Ni and Al atoms in the cluster, competition between maximizing Ni-Al and minimizing Ni-Ni interaction exists along with a preference for Al atom to segregate to the surface.

Our analysis of the icosahedral-based motifs of the isomers of Ni_9Al_3 and $\text{Ni}_{15}\text{Al}_5$ reveals that these structures have less number of Ni-Al bonds and more number of Ni-Ni bonds as compared with their ground-state geometry. The ground-state geometries of the clusters are clearly driven by the competing effects between Ni-Al and Ni-Ni bonds. The structures with less number of Ni-Ni bonds and at the same time large number of Ni-Al bonds are seen to be energetically lower, which gives rise to distorted, asymmetric, and amorphous geometries. As discussed by Calleja *et al.* and Bailey *et al.* the surface energy of Al being lower than that of Ni, Al atoms are located preferably on the surface of the cluster. At the same time Ni-Ni bonding is minimized to reduce the surface energy cost of expansion of the cluster. In the clusters of $\text{Ni}_{21}\text{Al}_7$ and $\text{Ni}_{24}\text{Al}_8$, the ground-state geometries are mostly driven by the minimum number of Al-Al bonds.

TABLE I. Binding energy (eV/atom) and spin gaps (eV) of the ground-state geometries of $\text{Ni}_{3n}\text{Al}_n$ clusters. V. Shah and D. G. Kanhere Table I.

System	B.E./atom	Energy gap (eV)	
		Spin-up	Spin-down
Ni_3Al	2.16	1.90	1.59
Ni_6Al_2	2.87	0.18	0.31
Ni_9Al_3	3.11	0.32	0.29
$\text{Ni}_{12}\text{Al}_4$	3.30	0.65	0.45
$\text{Ni}_{15}\text{Al}_5$	3.40	0.26	0.16
$\text{Ni}_{18}\text{Al}_6$	3.47	0.20	0.19
$\text{Ni}_{21}\text{Al}_7$	3.54	0.24	0.19
$\text{Ni}_{24}\text{Al}_8$	3.60	0.08	0.23
Bulk	5.04 ^a		

^aReference 37.

B. Electronic and Magnetic Properties

In order to understand the electronic properties, we have calculated the binding energy per atom (B.E.)/atom (in eV) and the energy gap (in eV) between the highest-occupied molecular orbital (HOMO) and lowest-unoccupied molecular orbital (LUMO) of spin-up and spin-down electrons, as a function of the size of the cluster. The binding energy per atom and the spin gaps are reported in Table I. The binding energy per atom increases monotonically as a function of the size of the cluster and is approaching the bulk cohesive energy limit of 5.04 eV.³⁷ The spin-up and spin-down electron gaps are highest for the smallest cluster of Ni_3Al . In all the remaining clusters, the gaps for spin-up and spin-down electrons are small and in the range of 0.008–0.7 and 0.14–0.44 eV, respectively. It is clearly seen that there is a decrease in the spin gaps with an increase in the size of the clusters. This signifies an increase in the metallic character of the $\text{Ni}_{3n}\text{Al}_n$ clusters with increasing size.

Figure 3 shows the charge-density isosurfaces of $\text{Ni}_{3n}\text{Al}_n$, ($n=1, 8$) clusters plotted at an isovalue of 0.3. A detailed analysis of the charge densities shows that the *d* band is not completely filled in all these clusters. There is a charge transfer from the *s* orbital of Ni to the *p* orbital of Al. In addition, there is also a charge transfer from *s* orbital of Al to *p* orbital of Al. This leads to a net gain in *p* charge of Al and a net loss in *s* charge of Ni. The amount of charge transferred from *s* orbital of Ni to *p* orbital of Al is increasing with the size of the clusters. This kind of a charge transfer from Ni to Al has also been seen in NiAl bulk.³⁸ The sharp *s-p* features disappear on account of mixing with *d* orbitals and an increase in *3d* delocalization is observed with increase in the overlap of *3d* orbitals.

The density of states of spin-up and spin-down electrons in $\text{Ni}_{3n}\text{Al}_n$, ($n=1, 8$) clusters are plotted in Fig. 4. Positive values are of spin-up electrons and negative values indicate spin-down electrons. The Fermi energy is shown by a vertical line in the individual density-of-states plots. In all the clusters, the density of states of the spin-up and spin-down

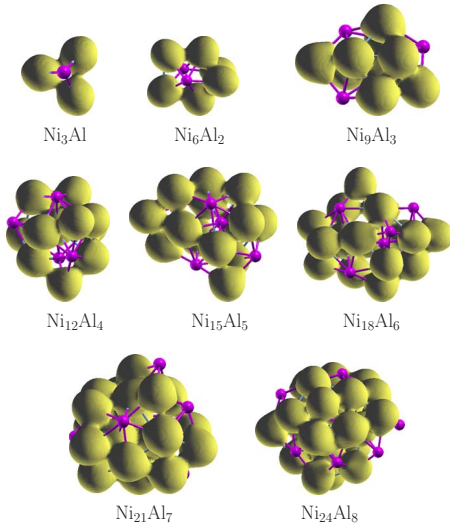


FIG. 3. (Color online) Charge-isodensity surfaces of the ground-state structures of $Ni_{3n}Al_n$ clusters. The purple spheres are Al atoms.

electrons are similar. The s and p states are prominently seen only in the smallest cluster of Ni_3Al . In all the clusters, the most dominant peak is that of the Ni d states, and the d states are gradually broadening with an increase in the size of the clusters, as shown in Table II. This is because of the increase in the number of Ni atoms as the size of these clusters increases. We would also like to point out that as the size of the clusters increases the difference in the spin-up and spin-down states is reducing from the lowest states. This indicates that in larger clusters, the magnetic moments are essentially due to the small number of states near the HOMO. Whereas, for small clusters the contribution to the magnetic moments extends to states well below the HOMO.

One noticeable feature in all the clusters is the partially empty d states at the Fermi level. Table III lists the density of states in the spin-up and spin-down channels at the Fermi level. All the clusters (except Ni_3Al) show higher occupancy in the spin-down channel as compared to that of spin-up channel. This has interesting consequences for electrical conduction. The density of states in the spin-down channel is seen to increase with the cluster size. The conductance in these clusters is a size-dependent feature. The conductance will be enhanced with increasing size. We note that these clusters exhibit half-metallicity that is somewhat different from the Heusler alloys, where, conduction is via one spin channel, which is completely polarized. The conductance in these clusters will be via electrons that have either kind of polarization, however, majority of the carriers will have a spin-down polarization.

The calculated contribution of the d electrons to the magnetic moment, total magnetization, the magnetic moment per atom, and the width of spin-up d states of the ground-state structures of $Ni_{3n}Al_n$, ($n=1, 8$) clusters are listed in Table II. The spin-down d states show similar widths, and hence are not listed. The results demonstrate that the significant contribution to the total magnetic moment of the clusters is from the d electrons. Table II shows that the smallest cluster has the largest magnetic moment per atom. The total magnetic

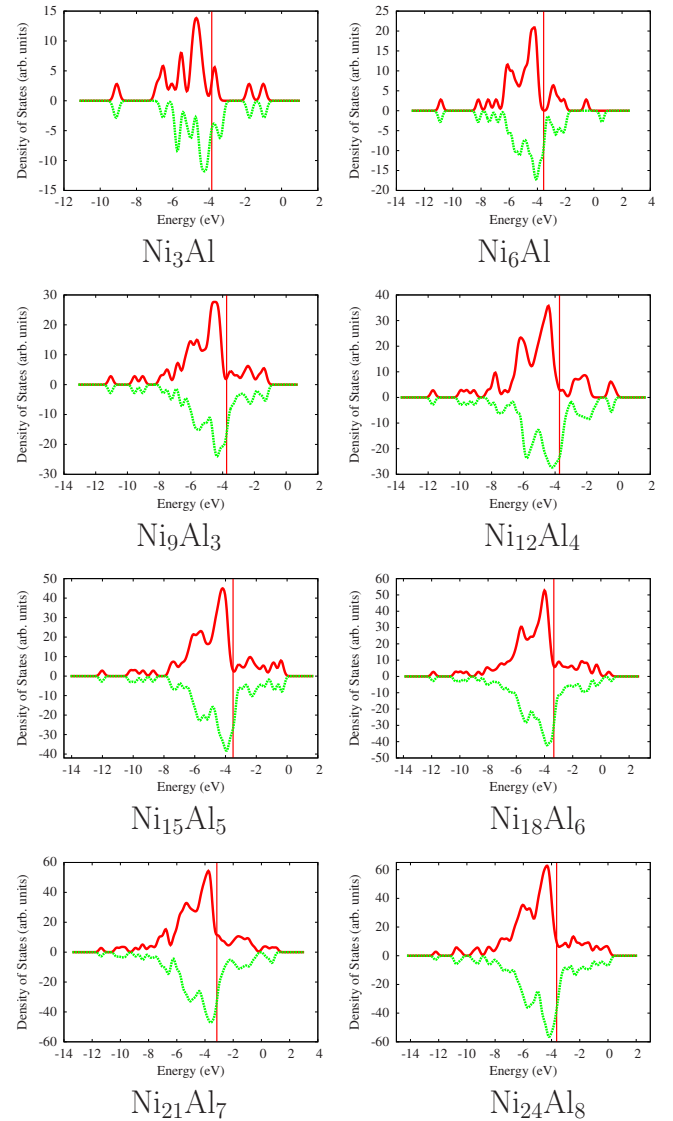


FIG. 4. (Color online) The spin-up and spin-down density of states of $Ni_{3n}Al_n$ clusters. The spin-up density of states is shown in the upper panel and the spin-down density of states is shown in the lower panel. The Fermi energy level of each cluster is shown by a vertical line. The energy gaps can be seen in Fig. 5.

moment per atom in the clusters is enhanced in comparison with the bulk magnetic moment per atom. Ni_3Al bulk is known to be a weak ferromagnet, however, the magnetic moments in $Ni_{3n}Al_n$ clusters are enhanced by an order of magnitude. The total magnetic moment increases with an increase in the size of the cluster. The width of the spin-up d states and spin-down d states (not listed here) is increasing with the size of the cluster and is a result of the delocalization of electrons as seen in Figs. 4 and 5. The magnetic moment per atom is reducing with the increasing size of the cluster and is approaching the bulk magnetic moment per atom. Our calculated bulk magnetic moment is in agreement with that reported by Guo *et al.*³⁹ The approach of the cluster magnetic moments to the bulk magnetic moment, with increasing cluster size, however, is not smooth. Duan *et al.* obtained using density functional theory the magnetic mo-

TABLE II. d orbital contribution to the magnetic moment, the total magnetization, the magnetization per atom (μ_B) and the width of the spin-up d states (in eV) of the ground-state structures of $Ni_{3n}Al_n$ clusters. V. Shah and D. G. Kanhere Table II

System	D	Total	μ_B	$dw \uparrow$ (eV)
Ni_3Al	1.77	1.66	0.41	4.33
Ni_6Al_2	2.22	2.04	0.37	6.39
Ni_9Al_3	3.37	3.23	0.27	6.40
$Ni_{12}Al_4$	5.61	5.65	0.35	6.98
$Ni_{15}Al_5$	5.29	4.93	0.25	7.66
$Ni_{18}Al_6$	5.54	5.32	0.22	7.68
$Ni_{21}Al_7$	6.55	6.32	0.22	7.31
$Ni_{24}Al_7$	7.81	7.58	0.24	7.64
Bulk			0.18	

ments per atom of small Ni clusters. Their calculations show that in pure Ni clusters the magnetic moments show an oscillatory behavior and for clusters of 5–15 atoms the magnetic moments reduce from 1.8 to $0.6 \mu_B$, whereas, for clusters of 17–32 atoms the magnetic moments reduce from 1.2 to $0.8 \mu_B$.¹⁸ Our calculated magnetic moments in Table II are small in comparison with the magnetic moments of pure Ni clusters. In the smallest cluster of Ni_3Al , with only one Al atom in the cluster, the magnetic moment is already considerably quenched. Thus, the presence of Al atoms tends to reduce the magnetic moment per atom of the clusters.

The energy-level distribution of the spin-up and spin-down states is shown in Fig. 5 for the $Ni_{3n}Al_n$, ($n=1,8$) clusters. For each cluster, the energy levels on the left-hand side of the plot show the spin-up states and the energy levels on the right-hand side show the spin-down states. The blue horizontal line shows the Fermi energy level. All the clusters show the spin-down energies to be shifted up in comparison with the spin-up energies. The small clusters with the highest magnetic moments, Ni_3Al , Ni_6Al_2 , Ni_9Al_3 , and $Ni_{12}Al_4$ show localized spin-up and spin-down energy levels. In all these clusters, the number of like and unlike atom neighbors of Ni and Al is much small in comparison with the bulk coordination number. In bulk Ni_3Al , each Ni atom has eight like nearest neighbors and four unlike nearest neighbors,

TABLE III. The total density of states of the spin-up and spin-down electrons at the Fermi level of $Ni_{3n}Al_n$ clusters. V. Shah and D. G. Kanhere Table III.

System	dos \uparrow	dos \downarrow
Ni_3Al	3.7	3.7
Ni_6Al_2	0.7	9.2
Ni_9Al_3	2.5	17.9
$Ni_{12}Al_4$	3.2	23.8
$Ni_{15}Al_5$	0.8	32.2
$Ni_{18}Al_6$	6.7	31.4
$Ni_{21}Al_7$	11.5	32.9
$Ni_{24}Al_7$	1.0	37.7

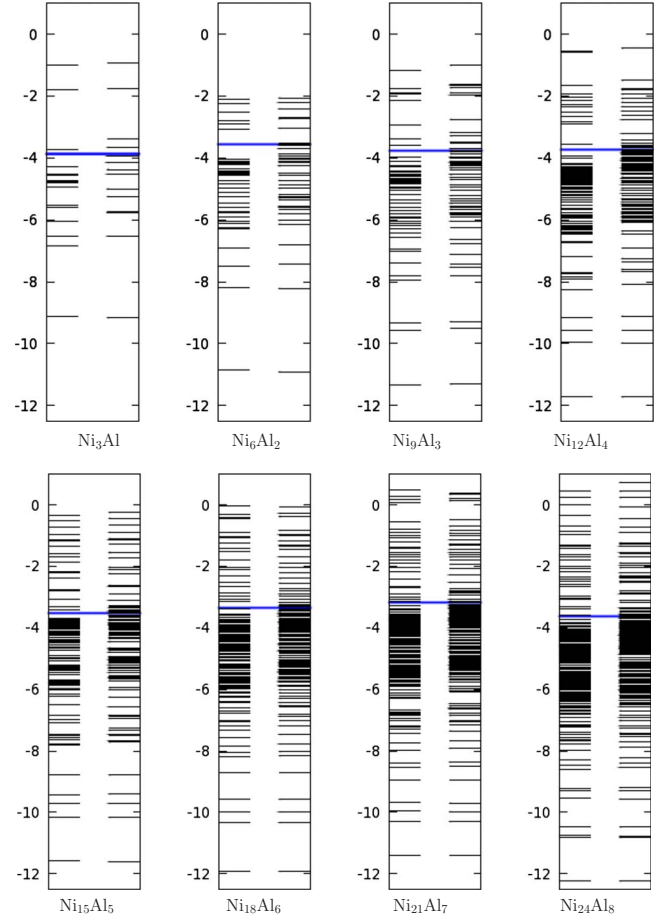


FIG. 5. (Color online) The energy level diagram of the $Ni_{3n}Al_n$ clusters. The distribution of the spin-up energy levels is shown on the left-hand side and the distribution of the spin-down energy levels is shown on the right-hand side for each cluster. The Fermi energy level of each cluster is marked by a blue horizontal line.

whereas, each Al atom has 12 unlike nearest neighbors only. The reduced coordination in small clusters of $Ni_{3n}Al_n$ leads to localization of d levels, which reflects in the enhanced magnetic moments of these clusters. For clusters of $Ni_{15}Al_5$ to $Ni_{24}Al_8$ the number of unlike atom neighbors and the like atom neighbors are increasing toward the bulk Ni_3Al coordination numbers. This increased coordination increases the overlap of the d orbitals, delocalizing the spin-up and spin-down energy levels, leading to a quenching of the magnetism in these clusters, as seen in solids.

To understand the distribution of magnetization density on the Ni and Al atoms in the $Ni_{3n}Al_n$, ($n=1,8$) clusters, we have shown in Fig. 6, the spin-density $[\rho^\uparrow - \rho^\downarrow]$ isosurfaces at $0.1 e/\text{\AA}^3$. The isosurface of spin density is localized on Ni sites only, however, the Ni atoms do induce a weak magnetization on the nearest Al atoms. In Ni_3Al , the spin density is distributed equally on the three Ni atoms. This is the only cluster, where all Ni atoms have an equal distribution of magnetic charge, on account of having an equal coordination with Al and Ni atoms. The magnetic distribution on Ni_6Al_2 shows a small negative magnetic moment of $-0.051 \mu_B$ on the Al atoms. The spin density is unequally distributed on the Ni atoms with the magnetic moments in the range of

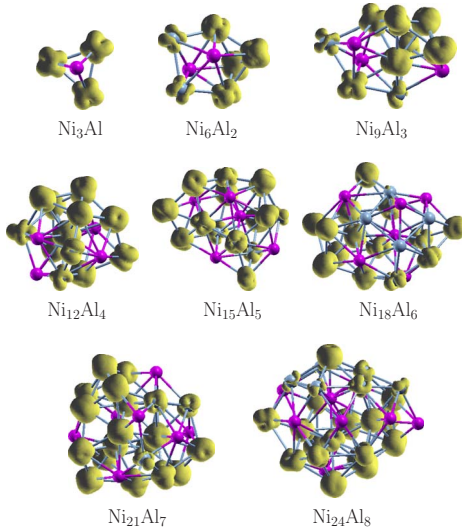


FIG. 6. (Color online) Constant positive spin density surfaces of the ground-state structures of $\text{Ni}_{3n}\text{Al}_n$ clusters corresponding to $0.1 e\text{\AA}^{-3}$. Grey spheres represent Ni atoms and purple spheres represent Al atoms.

$\sim 0.4\text{--}0.5 \mu_B$ on the four atoms that have a higher coordination with other Ni atoms. The remaining two Ni atoms have magnetic moment of $0.2 \mu_B$.

The Al atoms in Ni_9Al_3 have small negative magnetic moment of 0.03 and $0.04 \mu_B$. The distribution of magnetic moments on Ni atoms is seen to be unequal, ranging all the way from 0.2 to $0.6 \mu_B$. The distribution of positive magnetic moments on the Ni atoms in $\text{Ni}_{12}\text{Al}_4$, $\text{Ni}_{15}\text{Al}_5$, and $\text{Ni}_{21}\text{Al}_8$ is again inhomogeneous, ranging from $0.2\text{--}0.7, 0.06\text{--}0.6$, and $0.1\text{--}0.5 \mu_B$, respectively. In all these clusters, there is a small induced negative magnetic moment of $0.01\text{--}0.04 \mu_B$ on the Al atoms and one Al atom is seen to have a negligible magnetic moment in $\text{Ni}_{12}\text{Al}_4$ and $\text{Ni}_{21}\text{Al}_8$. In $\text{Ni}_{15}\text{Al}_5$, two Al atoms have $-0.02 \mu_B$ and three Al atoms have $-0.04 \mu_B$ magnetic moments. The clusters of $\text{Ni}_{18}\text{Al}_6$ and $\text{Ni}_{24}\text{Al}_8$ are interesting, with some Ni atoms showing negligible positive or negative magnetic moments. In $\text{Ni}_{18}\text{Al}_6$, the magnetic moments of Al atoms vary from $0.005\text{--}0.03 \mu_B$ and there are four Ni atoms with $0.003, 0.02, 0.03$, and $-0.05 \mu_B$ magnetic moments, respectively. The largest magnetic moment on Ni atoms in this cluster is $0.6 \mu_B$. In $\text{Ni}_{24}\text{Al}_8$, there are three Ni atoms with $0.08, 0.09$, and $0.1 \mu_B$ magnetic moments, respectively. The magnetic moments on the rest of the Ni atoms in both these clusters are highly inhomogeneous and range from $0.2\text{--}0.6 \mu_B$. One Al atom has a negligible magnetic moment of $-0.005 \mu_B$. The induced magnetic moment on the Al atoms in these clusters is similar to that seen in clusters of $\text{Ni}_{12}\text{Al}_4$, $\text{Ni}_{15}\text{Al}_5$, and $\text{Ni}_{21}\text{Al}_8$. Each Ni and Al atom in these clusters has a different number of like and unlike neighbors which results in different magnetic moments on individual atoms.

In general, in all these clusters, we observe that the Al atoms show small induced magnetic moments. The distribution of magnetic moments on Al and Ni atoms is significantly inhomogeneous. An analysis of the geometries of these clusters shows that the Ni atoms with very small mag-

netic moments (positive or negative) have an approximately equal proportion of the number of Ni neighbors and Al neighbors. The Ni atoms with more number of Ni neighbors, in comparison with Al neighbors, tend to have large magnetic moments. The magnetic spin density on Ni atoms is directed perpendicular to the surface of the cluster. Our results bring out that the magnetization distribution on the Ni atoms is inhomogeneous and depends on the local environment of the atoms (i.e., the number of Ni and Al neighbors as well as the positions of the Al neighbors with respect to the Ni atoms). The magnetic moments of Ni atoms are not dependent on the location of the Ni atom, i.e., at the center or on the surface of the cluster. The magnetic moment of Ni atom is high, if it has more Ni neighbors and less Al neighbors, and *vice versa*. We would like to note that although the nearest-neighbor atom model helps to understand the origin of inhomogeneity in the magnetic moments of the Ni atoms, the relative strength of the magnetic moments cannot be solely predicted on the basis of this model. The magnetic moment of atoms is sensitive to the local environment of the atoms and their neighbors in the cluster.

IV. CONCLUSION

The present work reports the structure, electronic and magnetic properties of $\text{Ni}_{3n}\text{Al}_n$ clusters based on *ab initio* total-energy calculations. Except for the smallest cluster of Ni_3Al , the ground-state geometries are asymmetric, distorted, and amorphous. The structures of $\text{Ni}_{3n}\text{Al}_n$, ($n=5, 8$) clusters show complete disagreement with the structures obtained by Gupta potential. Clear patterns of evolution based on a double icosahedral motif are not evident. However, the structures are cage-like, and comprised of distorted pentagonal and hexagonal rings. The amorphous structures of these clusters suggest that the thermodynamic and melting properties of the clusters will be significantly different than those observed in pure Ni or Al clusters.

The charge-density analysis shows that there is no significant difference in the spin gaps or general nature of density of states of the spin-up and spin-down electrons. The spin-up states are very slightly occupied at the Fermi level. The spin-down states show an increase in occupancy with an increase in the size of the clusters. The conduction properties of such clusters will depend on the size of the cluster, and an enhancement in conduction with increasing size of the clusters may be observed. It would be interesting to verify this through experimental investigations.

The magnetic moments are enhanced in these clusters in comparison with bulk and preference of center or surface atoms for large magnetization densities is not evident. Atoms with more number of Ni neighbors, in comparison with Al neighbors, are seen to carry large spin densities. Atoms with an almost equal number of Ni and Al neighbors tend to have the smallest spin densities. Inhomogeneous distribution of positive spin density on Ni atoms and negative spin densities on Al atoms is observed.

Our results on the $\text{Ni}_{3n}\text{Al}_n$ clusters indicate that the empirical potentials like Gupta potentials that have been fitted to the properties of bulk materials may not lead to reliable

results in small nanoclusters. We believe, that in such nanoclusters, where compositions of the elements are not in the impurity range or low level of doping, the size range of the applicability of these potentials needs to be critically investigated before applying them to such studies. There is clearly a need of better empirical potentials for small bimetallic alloy clusters. We believe that incorporation of first-principles data of small systems in the fitting database may significantly improve the reliability of such potentials, not only for small systems, but also for bulk materials.

ACKNOWLEDGMENTS

V.S. is grateful to R. Balamuralikrishnan and S. Sankarabramanian for helpful discussions on nickel-based superalloys. Defense Metallurgical Research Laboratory, Hyderabad is gratefully acknowledged for funding this work. V.S. would also like to acknowledge the funding support from Department of Science and Technology, India and University of Pune. V.S. acknowledges the genial hospitality of the Bioinformatics Centre, University of Pune during the course of this work.

*Corresponding author. Present address: Interdisciplinary School of Scientific Computing, University of Pune, Pune 411007; vaishali@unipune.ernet.in

- ¹F. Baletto and R. Ferrando, *Rev. Mod. Phys.* **77**, 371 (2005).
- ²C. T. Liu, C. L. White, and J. A. Horton, *Acta Metall.* **33**, 213 (1985).
- ³*Physical Metallurgy*, edited by R. W. Cahn and P. Haasen (Elsevier/North-Holland, Amsterdam, 1996), Vol. 3.
- ⁴Y. Mishin, *Acta Mater.* **52**, 1451 (2004).
- ⁵C. Rey, J. Garcia-Rodeja, and L. J. Gallego, *Phys. Rev. B* **54**, 2942 (1996).
- ⁶E. B. Krissinel and J. Jellinek, *Chem. Phys. Lett.* **272**, 301 (1997).
- ⁷E. B. Krissinel and J. Jellinek, *Int. J. Quantum Chem.* **62**, 185 (1997).
- ⁸E. F. Rexer, J. Jellinek, E. B. Krissinel, E. K. Parks, and S. J. Riley, *J. Chem. Phys.* **117**, 82 (2002).
- ⁹E. K. Parks, E. F. Rexer, and S. J. Riley, *J. Chem. Phys.* **117**, 95 (2002).
- ¹⁰M. Calleja, C. Rey, M. M. G. Alemany, L. J. Gallego, P. Ordejón, D. Sánchez-Portal, E. Artacho, and J. M. Soler, *Phys. Rev. B* **60**, 2020 (1999).
- ¹¹E. Viitala, H. Häkkinen, M. Manninen, and J. Timonen, *Phys. Rev. B* **61**, 8851 (2000).
- ¹²M. C. Michelini, R. P. Diez, and A. H. Jubert, *Int. J. Quantum Chem.* **70**, 693 (1998).
- ¹³N. Rosch, L. Ackermann, and G. Pacchioni, *Chem. Phys. Lett.* **199**, 275 (1992).
- ¹⁴S.-R. Liu, H.-J. Zhai, and L.-S. Wang, *Phys. Rev. B* **65**, 113401 (2002).
- ¹⁵S. E. Apsel, J. W. Emmert, J. Deng, and L. A. Bloomfield, *Phys. Rev. Lett.* **76**, 1441 (1996).
- ¹⁶S. Bouarab, A. Vega, M. J. López, M. P. Iñiguez, and J. A. Alonso, *Phys. Rev. B* **55**, 13279 (1997).
- ¹⁷F. Aguilera-Granja, S. Bouarab, M. J. López, A. Vega, J. M. Montejano-Carrizales, M. P. Iñiguez, and J. A. Alonso, *Phys. Rev. B* **57**, 12469 (1998).
- ¹⁸H. M. Duan, X. G. Gong, Q. Q. Zheng, and H. Q. Lin, *J. Appl. Phys.* **89**, 7308 (2001).
- ¹⁹C. J. M. Castro and D. R. Salahub, *Chem. Phys. Lett.* **271**, 133 (1997).
- ²⁰F. A. Reuse and S. N. Khanna, *Chem. Phys. Lett.* **234**, 77 (1995).
- ²¹B. V. Reddy, S. K. Nayak, S. N. Khanna, R. K. Rao, and P. Jena, *J. Phys. Chem. A* **102**, 1748 (1998).
- ²²R. Ahlrichs and S. D. Elliott, *Phys. Chem. Chem. Phys.* **1**, 13 (1999).
- ²³M. C. Michelini, R. P. Diez, and A. H. Jubert, *J. Mol. Struct.: THEOCHEM* **490**, 181 (1999).
- ²⁴W. Zhang, W.-C. Lu, J. Sun, C. Wang, and K. Ho, *Chem. Phys. Lett.* **455**, 232 (2008).
- ²⁵H.-P. Cheng, R. S. Berry, and R. L. Whetten, *Phys. Rev. B* **43**, 10647 (1991).
- ²⁶X. G. Gong, D. Y. Sun, and X.-Q. Wang, *Phys. Rev. B* **62**, 15413 (2000).
- ²⁷T. H. Upton, *Phys. Rev. Lett.* **56**, 2168 (1986).
- ²⁸H. Fengyou, Z. Yongfang, L. Xinying, and L. Fengli, *J. Mol. Struct.: THEOCHEM* **807**, 153 (2007).
- ²⁹M. S. Bailey, N. T. Wilson, C. Roberts, and R. L. Johnston, *Eur. Phys. J. D* **25**, 41 (2003).
- ³⁰Y. H. Yao, X. Gu, M. Ji, X. G. Gong, and D.-s. Wang, *Phys. Lett. A* **360**, 629 (2007).
- ³¹S. H. Yang, D. A. Drabold, J. B. Adams, and A. Sachdev, *Phys. Rev. B* **47**, 1567 (1993).
- ³²G. Kresse and J. Furthmüller, Vienna *ab initio* simulation package (1996).
- ³³D. Vanderbilt, *Phys. Rev. B* **41**, 7892 (1990).
- ³⁴*Structure Data of Elements and Intermetallic Phases*, edited by K.-H. Hellwege, Landolt-Börnstein, New Series, Group III, Vol. 6 (Springer-Verlag, Berlin, 1971).
- ³⁵J. Rifkin, computer code XMD (University of Connecticut, 2004).
- ³⁶F. Cleri and V. Rosato, *Phys. Rev. B* **48**, 22 (1993).
- ³⁷V. Shah and R. Balamuralikrishnan (unpublished).
- ³⁸S. C. Lui, J. W. Davenport, E. W. Plummer, D. M. Zehner, and G. W. Fernando, *Phys. Rev. B* **42**, 1582 (1990).
- ³⁹G. Y. Guo, Y. K. Wang, and L.-S. Hsu, *J. Magn. Magn. Mater.* **239**, 91 (2002).